Assessment of shrinkage and bond behaviour of high performance cement-based composites as a repair mortar

Baloch, Hassan; Grünewald, Steffen; Matthys, Stijn

DOI
10.1016/j.dibe.2023.100203

Publication date
2023

Document Version
Final published version

Published in
Developments in the Built Environment

Developments in the Built Environment 15 (2023) 100203

Contents lists available at ScienceDirect

Developments in the Built Environment

journal homepage: www.sciencedirect.com/journal/developments-in-the-built-environment

Assessment of shrinkage and bond behaviour of high performance cement-based composites as a repair mortar

Hassan Baloch [a,*], Steffen Grünewald [a,b], Stijn Matthys [a]

[a] Magnel-Vandepitte Laboratory, Department of Structural Engineering and Building Materials, Ghent University, Ghent, Belgium
[b] Engineering Structures, Delft University of Technology, Stevinweg 1, Delft, 2628 CN, the Netherlands

ARTICLE INFO

Keywords:
Strain-hardening cementitious composites
SHCC
Shrinkage
Mortar
Repair
Strengthening
Cracking
Restraint factor

ABSTRACT

There is a need to develop innovative repair materials which can overcome the challenges of cement-based repair mortars being relatively prone to shrinkage effects. In practice, free shrinkage of repair mortar is often considered as an indicator for potential cracking and delamination of applied repair mortars due to restrained shrinkage effects. As it is hard to measure restrained shrinkage directly, a restraint factor (R) can be used to correlate both. This study investigates the shrinkage characteristics of strain-hardening cementitious composites (SHCC), making use of polyvinyl-alcohol (PVA), high-density poly-ethylene (HDPE), or short glass fibres, for the repair and strengthening of existing concrete structures. Along with drying shrinkage and autogenous shrinkage, restrained shrinkage has been characterized with respect to the concrete substrate. Furthermore, pull-off tests were performed to assess the bond properties of these repair mortars. The results show around 65% higher autogenous shrinkage in high strength SHCC mixes while there was a decrease in drying shrinkage compared to the reference mix. In contradiction to what was initially expected, an increase in fibre content from 1.5 to 2.0 vol % resulted in a significant increase in autogenous shrinkage, especially in the high strength SHCC mixes. The restraint factor for all repair mortars was determined and was found to be in the range of 0.82–0.94. The pull-off tests showed an overall excellent bond behaviour of all studied mortars.

1. Introduction

Reliable repair and strengthening of existing concrete structures is a worldwide challenge considering the high complexity, the importance of using compatible material systems with good bond performance to the existing substrate, and costs involved of the contemporary concrete repair methods. According to statistics, renovation costs account for 50% of the total construction budget both in United States and Europe (Koch et al., 2002; Fan et al., 2022). Frequent issues which make it necessary to rehabilitate existing structures include changes in the use of the structure, for example, higher and/or more frequent loading, ageing of concrete, and reduction of load carrying capacity of the structure due to errors in the design or during construction (Scheerer et al., 2018; Yang et al., 2021). Keeping these challenges in mind, there is a need to develop innovative materials and technologies for the repair and strengthening of existing structures.

Strain-hardening cementitious composites (SHCC) is a novel high-performance fibre-reinforced cementitious composite that is designed by applying the concepts of micromechanics (Ranade et al., 2013; Curosu et al., 2022). This allows the optimization of composites, so that under tensile and bending loads they generate multiple fine cracks. These properties are usually achieved by the addition of short synthetic fibres which bridge the cracks, resulting in high fracture toughness and reduced crack width (Li, 2003). Using high performance fibres such as poly-vinyl alcohol (PVA) and high-density polyethylene (HDPE), it is also possible to reach tensile strengths of up to 15 MPa, further to a strain capacities of larger than 4% (Yu et al., 2017). These properties make SHCC advantageous both for new structures and strengthening of existing concrete structures. SHCC has been used as a repair material for both flexure strengthening (Khan et al., 2022) and shear strengthening (Yang et al., 2021) of reinforced-concrete structures. SHCC also has high physical and chemical compatibility with the concrete substrate and can be applied in thin layers with a small increase in weight (Do Yun, 2013). The narrow crack widths of the SHCC is also regarded as beneficial for the durability of the repaired elements (Van Zijl et al., 2012; Mechtcherine, 2012; Zukowski et al., 2018).

Often, SHCC is produced using short polyvinyl-alcohol (PVA) fibres at a dosage of 2.0 vol.-% (Li, 2003; Mechtcherine et al., 2011). These

* Corresponding author.
E-mail address: hassan.baloch@ugent.be (H. Baloch).

https://doi.org/10.1016/j.dibe.2023.100203
Received 8 June 2023; Received in revised form 16 July 2023; Accepted 23 July 2023
Available online 25 July 2023

fibres have a hydrophilic nature which means that they develop a very strong chemical bond with the surrounding cement matrix. To avoid pre-mature fibre rupture during crack propagation, the fibre-matrix interfacial bond is limited by replacing a significant amount of cement with fly ash in combination with a relatively high water-binder ratio. These measures lead to average mechanical properties and a higher permeability (Curosu et al., 2017), yet excellent strain hardening (dispersed cracking) effect. Recently, fibres made with HDPE are used to produce high strength SHCC because of their superior mechanical and physical properties. In contrast to PVA fibres, HDPE fibres are hydrophobic in nature and have a high elastic modulus of elasticity and tensile strength. These features allow the development of a high-strength compact cementitious matrix which are achieved by considerably increasing the cement content and by reducing the water-binder ratio. To increase the packing density of such high strength mixes, silica fume is used as a binder and replacement of cement in combination with a lower amount of fine quartz sand (Mechtcherine et al., 2011; Baloch et al., 2021).

The usage of short glass fibres is more common since the advent of alkali-resistant high performance glass fibres, especially for shotcrete repair mortars (Xu et al., 2021). These fibres also improve the tensile strength of the repair mortar and the ductility of the cementitious composites owing to their excellent mechanical properties (Ghugal and Deshmukh, 2005). However, with a generally low water-binder ratio and the inclusion of reactive secondary raw materials such as silica fume, these repair materials can be prone to early-age cracking caused by autogenous shrinkage (Şahmaran et al., 2009). To successfully apply these novel cementitious materials for repair, it is necessary to consider the volumetric compatibility between the SHCC repair mortars and the concrete substrate.

In order to measure total and autogenous shrinkage of SHCC, prism like specimens are often applied (Wang et al., 2020; Xiong et al., 2021). Li (Li and Li, 2006) performed free shrinkage tests on PVA-SHCC, steel fibre reinforced concrete and plain concrete; and concluded that PVA-SHCC had the highest free shrinkage strain value due to higher cement content and no coarse aggregates. Wang & Li (Wang and Li, 2005) found the total shrinkage of PVA-SHCC to be 80% higher than that of concrete. Despite the higher shrinkage, this did not lead directly to large shrinkage crack widths, as was investigated using a ring test. The authors found only microcracks (<50 μm) in SHCC while for concrete one large crack appeared with crack width of 1 mm. The authors concluded that the total shrinkage of SHCC (<0.3%) is far below the tensile strain capacity, so that the mortar is still in strain-hardening stage contrary to most plain concretes.

The remaining shrinkage of the existing concrete substrate is relatively small due to the age of the substrate, while the placed repair mortar layer will still need to undergo the major part of its shrinkage. Given proper bond interaction between both materials, these differences in occurring shrinkage can affect the effectiveness of the repair system. Tensile stresses may be induced in the repair material when its volume changes are restricted by the concrete substrate. This effect is called 'restrained shrinkage', versus 'free shrinkage' in the absence of any restraint (Cheung and Leung, 2011). In reality, the deformation measured under restrained shrinkage situation is the actual strain ε_a and restrained shrinkage stresses in the structure are proportional to the difference between the measured shrinkage ε_a and the free shrinkage ε_f. This can be written in the form,

$$\varepsilon_r = \varepsilon_f - \varepsilon_a \quad (1)$$

where, ε_r is the restrained strain in the mortar. This restraining effect will result in shear stresses at the bond interface and in tensile stresses in the applied repair mortar. These stresses can be considered to be proportional to the restrained strain and modulus of elasticity of the applied mortar, and are partially reduced because of tensile relaxation (Beushausen and Bester, 2016). Equation (1) can also be written in terms of a restraint factor R which takes the form

$$\varepsilon_r = R\,\varepsilon_f \quad (2)$$

$$\varepsilon_a = (1 - R)\varepsilon_f \quad (3)$$

If there is no restraint R = 0 and hence $\varepsilon_r = 0$ and $\varepsilon_a = \varepsilon_f$, while if the specimen is fully restrained R = 1, implying $\varepsilon_r = \varepsilon_f$ and $\varepsilon_a = 0$.

In literature, the restrained shrinkage behaviour of repair mortars has been investigated by employing a traditional ring-type test to measure the restrained shrinkage and observe the cracking of repair mortars (Hamedanimojarrad et al., 2012; Golias et al., 2012). This test gives some useful insights such as time to cracking of the material, but the outcome does not provide a direct correlation with free shrinkage. Also, this test does not simulate the actual restraining conditions when the repair mortar is applied on a concrete substrate. This study aims at bridging these research gaps by proposing a more realistic restrained shrinkage measuring method and also evaluating the correlation between free and restrained shrinkage of these high performance repair mortars.

2. Experimental program

2.1. Selected SHCC mix types and mixing procedure

An experimental program, comprising six formulations (see Table 1, including mix/specimen designation), was developed to investigate the shrinkage and bond properties of ordinary and high strength SHCC, applying 3 types of fibres (PVA, glass, HDPE; Fig. 1) and 2 types of fibre dosage (1.5 and 2.0 vol%). The SHCC mix formulations of the selected mixes are given in section 2.3 and resulted from initial mix design trials (Baloch et al., 2021).

A standard PVA SHCC mix by Wang and Li (2005) was selected as a reference with necessary revisions based on the available raw materials and type of super-plasticizer. Considering the hydrophilic nature of PVA fibres, a sufficiently high w/b ratio of 0.3 was applied. In order to avoid premature fibre rupture, a large portion of cement was replaced by fly ash to ensure mediocre mechanical and physical properties of the matrix. In order to study the effect of fibre type on shrinkage, the same mix parameters as for the PVA SHCC reference were also applied for a glass fibre based SHCC.

The high strength SHCC matrix was designed considering the optimal interaction with 20 mm thick and 12 mm long HDPE fibres. The HDPE SHCC mix was developed by increasing the cement content considerably (1100 kg/m^3) and by decreasing the w/b ratio to 0.22. Instead of fly ash, silica fume was used as cement replacement to increase the packing density of the mix.

The SHCC mix formulations as provided in Table 1 have been produced with a 2 litre mortar mixer (type Hobart). To have a homogeneous fibre dispersion in the mix, a total of 7-min mixing time was implemented. All dried constituents were first mixed for 1 min at 145 rounds per minute (rpm) followed by the addition of superplasticizer and water. Slow mixing at 145 rpm was then carried out for 3 min. Fibres were then added with 3 min of further fast mixing at 285 rpm. Fibres were added in batches to avoid the formation of fibre clumps during the mixing process.

Table 1
Mix formulations (kg/m^3).

Mix designation	Cement	Sand	Water	Fibre	Fly ash	Silica fume	SP
PVA1.5	540	470	365	19.5	665	–	4.5
PVA2	540	470	365	26	665	–	4.5
GL1.5	540	470	365	39	665	–	5
GL2	540	470	365	52	665	–	5
HDPE1.5	1100	450	285	15	–	190	21
HDPE2	1100	450	285	20	–	190	21

Fig. 1a. PVA fibres.

Fig. 1b. Glass fibres.

Fig. 1c. HDPE fibres.

Table 2
Properties of fibres used (values provided by manufactures).

Fibre type	Aspect ratio	Diameter (μm)	Length (mm)	Tensile Strength (MPa)	Modulus of elasticity (GPa)
PVA	307	39	12	1400	42.8
HDPE	600	20	12	2500	80
Glass	857	14	12	1500	72

Table 3
Chemical composition of cement, fly ash and silica fume (weight-%).

Oxide	CEM I	FA	SF
SiO_2	18.30	52.11	94.73
CaO	64.30	10.01	0.20
Al_2O_3	5.20	23.55	0.36
Fe_2O_3	4.00	7.32	0.71
$(Na_2O)_e$	0.32	4.52	0.20
MgO	1.40	4.09	0.39
SO_3	3.50	3.01	0.27
LOI	1.40	–	1.86
P_2O_5	–	3.12	–

2.2. Material properties

The properties of the applied fibres are given in Table 2, considering PVA (manufactured by Kuraray), glass (by Owens Corning Belgium) and HDPE (by DSM). The fibres are shown in Fig. 1. The cement used for both the substrate and the applied repair mortar was Portland cement type CEM I 52.5 N (by Holcim Belgium). Class F fly ash (FA) (by Vliegasunie) was used as a supplementary binder for the mixes based on PVA and glass fibres, while silica fume (SF) (by Elkem) was used for the mix with high strength HDPE fibres. The chemical composition of all the binders were determined by X-ray fluorescence and are given in Table 3. Fine silica sand type M34, (by Sibelco Belgium) has been used for all SHCC mixes, and has an average particle size of 174 μm. In order to improve the workability of the fresh SHCC, a polycarboxylate-based superplasticizer (Glenium 51, 35% con, BASF) was applied.

As concrete substrate for the SHCC repair mortar a concrete has been used with 455 kg/m^3 cement content , a water/cement ratio of 0.40 and maximum aggregate (rounded aggregate) size of 16 mm, resulting in an average 28 days compressive strength (cubes with side length 150 mm) of 62 MPa and an average tensile pull off strength to be 2.8 MPa.

2.3. Uniaxial tensile testing set-up

Uniaxial tests were performed on 3 dumbbell specimens per formulation, with dimensions as shown in Fig. 2, following the JSCE recommendations (Rokugo et al., 2007). The central part of the test specimen has a cross-section of 30 mm x 13 mm. Material was applied in wooden moulds, by scrapping the mortar over the mould surface in such a way to simulate repair mortar application. These moulds were covered with plastic foils and were stored in a curing chamber at T = 20 ± 2 °C, RH ≥

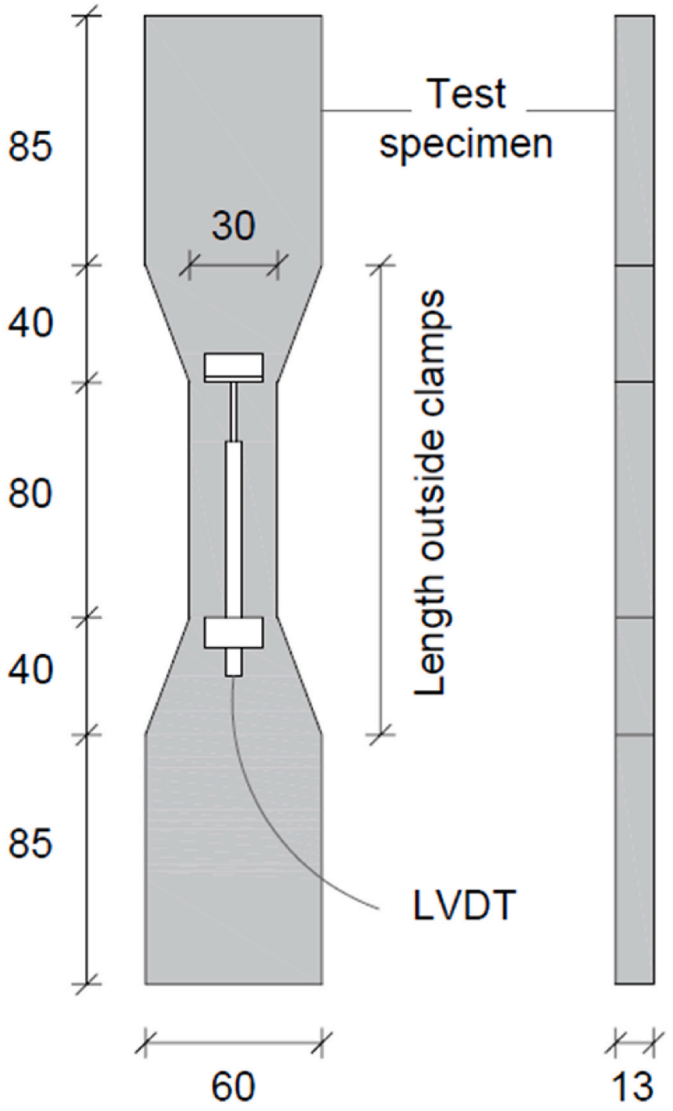

Fig. 2. SHCC dumbbell specimen (dimensions in mm).

95 %. The form was removed after 24 hours and the specimens were further cured in climate chamber at T = 20 ± 5 °C, RH = 65 ± 5 %. Uniaxial tests were performed at an age of 28 days under displacement control of 0.005 mm/s with a tensile testing machine with load capacity of 100 kN. During testing a linear variable displacement transducer (LVDT) was attached to one side of the specimen to measure the elongation (and associated tensile strain).

2.4. Total and autogenous shrinkage testing set-up

In order to have a comparable test configuration between restrained and free shrinkage measurements, repair mortar plates of 300x300x10 mm^3 (similar to the set-up described in Fig. 4) have been applied for monitoring total and autogenous shrinkage. The repair mortar was cast directly into pre-oiled wooden moulds and 6 specimens were prepared for each mix formulation. After 24 hours in the curing chamber (20 °C, ≥95 %RH), the formwork was removed, mechanical deformeter measurement points have been applied (in the same way as for the restrained shrinkage testing, Fig. 4), and strain measurements were executed daily for 28 days while the specimens where in the climate chamber (20 °C, 65 %RH). To measure autogenous shrinkage (starting after 24 hours), for each mix three plates were covered with an adhesive backed aluminium foil to avoid moisture loss. The specimens are shown in Fig. 3 (including

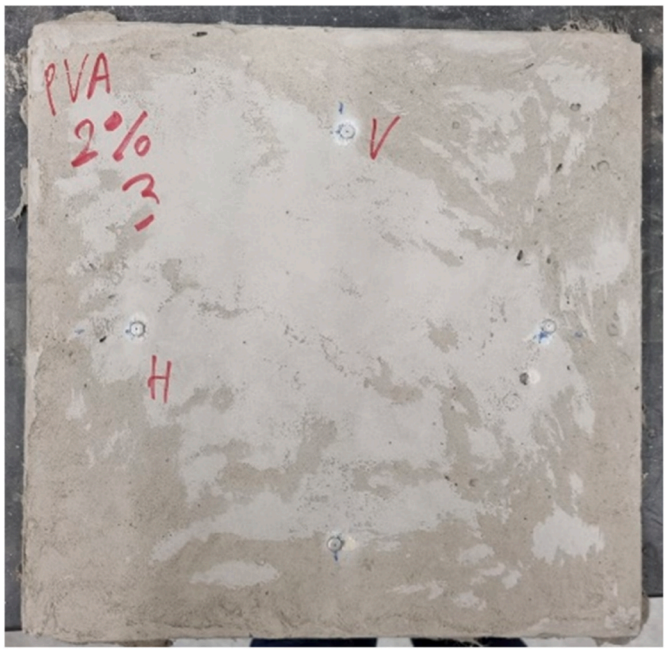

Fig. 3a. Total shrinkage plates.

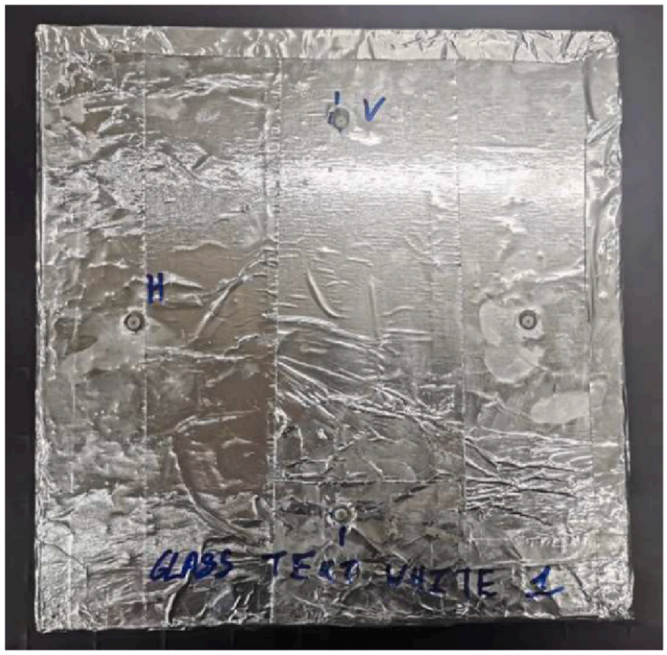

Fig. 3b. Autogenous shrinkage plates covered with aluminium sheets.

the cabinet that was used for the high number of specimens and whereby the specimens were mainly exposed to the atmosphere at the measured top side, while the soffit was resting on wooden planks).

2.5. Restrained shrinkage and pull-off bond testing set-up

Specimens for testing restrained shrinkage and pull-off bond strength were prepared according to EN 1542 (BS EN 1542, 1999). At least 2 specimens were tested for each formulation. The concrete substrate slabs of 300x300x100,mm^3 were cast, covered with plastic foil and stored in a climate chamber (20 °C, 65 %RH) for at least 3 months to minimize shrinkage with reference to repair mortar. The surface of the slabs was

Fig. 3c. Shrinkage plates storage.

grit blasted to a roughness index (Ri) of 0.45 mm. The surface roughness of the substrates was tested using the volumetric sand patch test method in accordance to EN 1766 (BS EN 1766, 2017).

Before application of the SHCC repair mortar, the substrate was prewetted for 30 min and patted dried to emulate saturated surface dry condition. Also the surface was cleaned with a steel brush to remove any excessive debris as per the EN 1542 (BS EN 1542, 1999). A 10 mm thick mortar overlay was chosen as mostly these special repair mortars are applied in thin layers (10–20 mm) (Wei et al., 2020) in practical repair executions. A wooden formwork was attached to the sides of the substrate slabs to ensure an equal thickness of 10 mm of the overlay and the repair mortar was carefully hand-applied in two consecutive placed layers. Specimens were then covered with plastic foil and stored in the curing chamber for 24 hours (20 °C, ≥95 %RH). After 24 hours, the wooden formwork was removed and the gauge length base points for mechanical deformeter measurements were attached at the surface as shown in Fig. 4 (a). The gauge length equals 200 mm. These specimens were then stored in the climate chamber (20 °C, 65 %RH) and restrained shrinkage was daily measured for 28 days in two directions

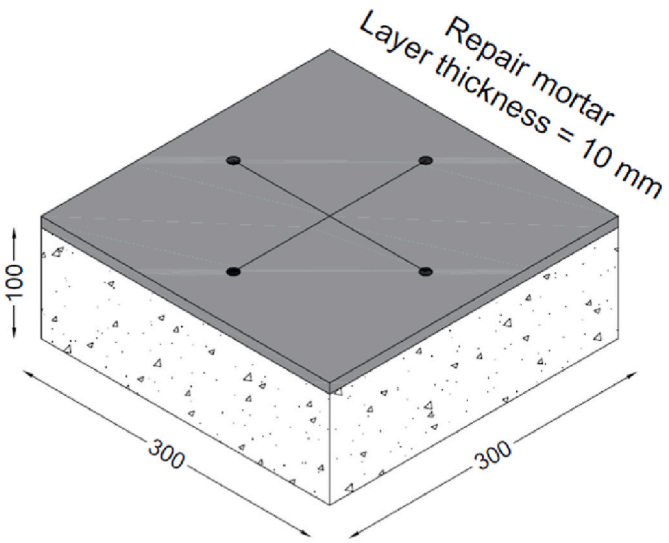

Fig. 4a. Restrained shrinkage specimen.

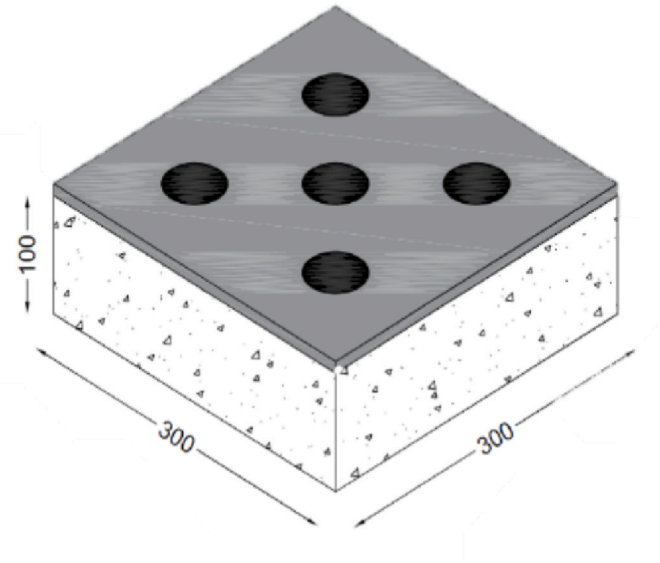

Fig. 4b. Points for pull-off bond testing.

perpendicular to each other at the centre of the specimens.

At the age of 28 days each specimen was subjected to five tensile pull-off tests in accordance with to EN 1542 (BS EN 1542, 1999). Hereby, for each specimen after 28 days, five circular cuts with a diameter of 50 mm were drilled with a diamond coring bit, about 15 mm into the substrate and according to the layout given in Fig. 4(c). Steel dollies (diameter 50 mm) are bonded using epoxy as structural adhesive, making sure that the epoxy is not entering the circular cuts, and allowing the epoxy to cure for about 12 h. At an age of 30 days of the SHCC overlay, the bond tests are performed with a direct pull-off bond testing device (type Proceq DY-2) at a continuous rate of 0.05 MPa/s until failure. Pull-off strength was finally calculated using the following equation.

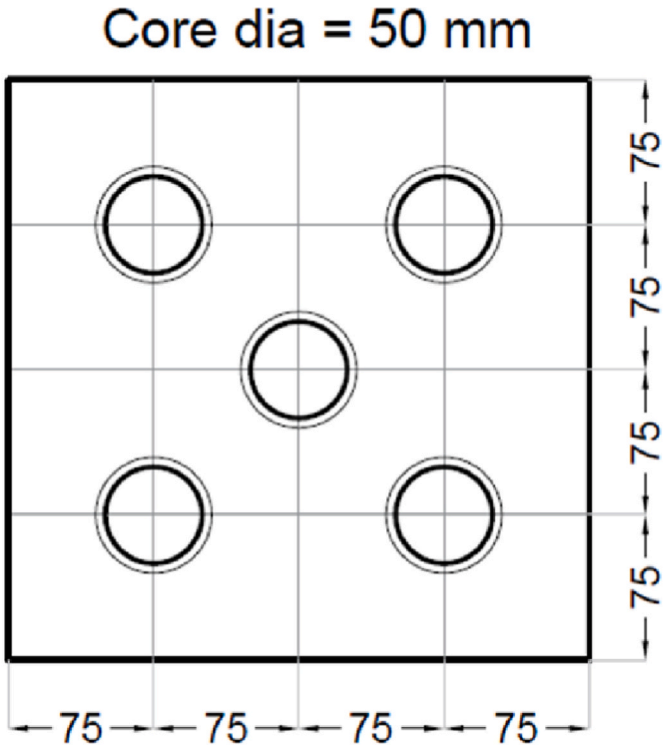

Fig. 4c. Pull-off discs layout.

$$f_h = \frac{4F_h}{\pi D^2} \quad (4)$$

Where f_h is the pull-off strength (N/mm^2), F_h is the failure load (N) and D is the mean diameter.

3. Results and discussion

3.1. Uniaxial tensile properties based on fibre type

Fig. 5 shows typical cracking pattern of the SHCC specimens, while Fig. 6 shows the stress-strain curves of repair mortars with 2% fibre content. The main test results (mean value of 3 specimens and standard deviation) are summarized in Table 4, in terms of stress at first cracking (σ_{1st}), maximum stress (σ_{max}), strain at maximum stress (ε_{max}), observed degree of strain hardening ($\sigma_{max}/\sigma_{1st}$), observed degree of distributed cracking, and ratio of maximum stress with respect to the PVA SHCC.

The tensile behaviour of specimen PVA2 is taken as a reference since PVA fibres are widely used to produce SHCC. The mix is categorized by an average ultimate tensile strength of 4.13 MPa and an average strain capacity of 1.8% The strain capacity of SHCC is categorized by the degree of multiple cracking and width of the cracks. Compared to the HDPE2, PVA2 yielded wider cracks with approximately 70 μm average residual crack width measured on post-tested samples. This value is almost twice as large than the high strength HDPE2 specimens. This is due to PVA having low Young's modulus that is almost half of the HDPE fibre.

Glass fibre SHCC mixes were the least ductile as strain capacity was significantly less at 0.15% (8.3% compared to the equivalent mix with PVA). There was no pronounced multiple cracking, as observed in the other mixes. The fracture surface of the specimens showed complete fibre rupture which indicates glass fibres for the tested mix demonstrated to have an excellent bond with the matrix causing the breakage of the fibres and hence localization of failure instead of multiple cracking. These fibres were also much stiffer compared to PVA and HDPE fibres and had a tendency to break even during the mixing process. The addition of glass fibres however increased the ultimate tensile strength of the matrix compared with PVA fibres and can be used in applications where high ductility is not required.

Comparing the high tensile strength SHCC (HDPE SHCC mix) with more normal tensile strength SHCC (PVA or glass fibre SHCC mix), indeed more high end properties are obtained for the HDPE SHCC. The average first crack stress value (σ_{1st}) of the HDPE mix was found out to be 4.6 MPa which is 42%higher than PVA2 fibre mix. Also the ultimate tensile strength (σ_{max}) of HDPE mixes were almost 100% higher than

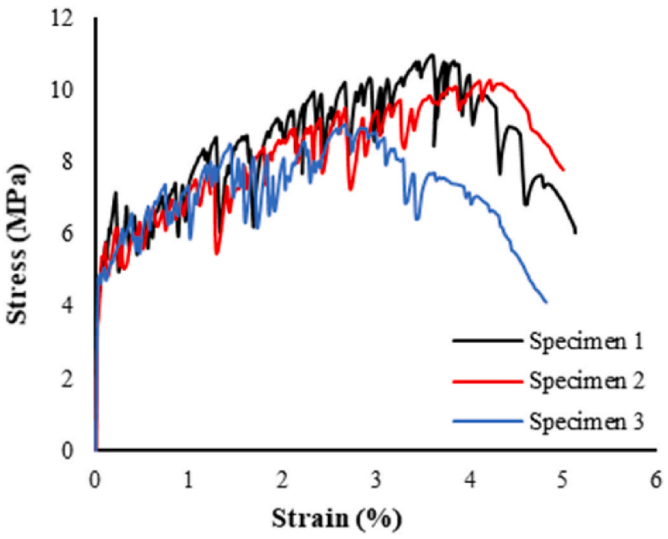

Fig. 6a. HDPE2.

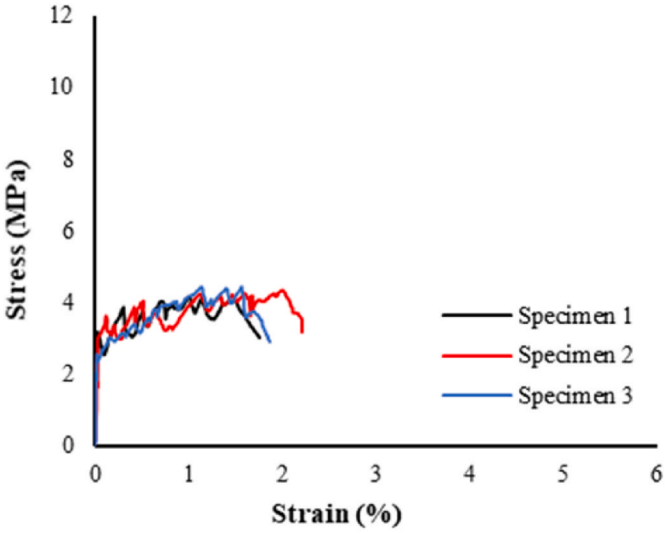

Fig. 6b. PVA2.

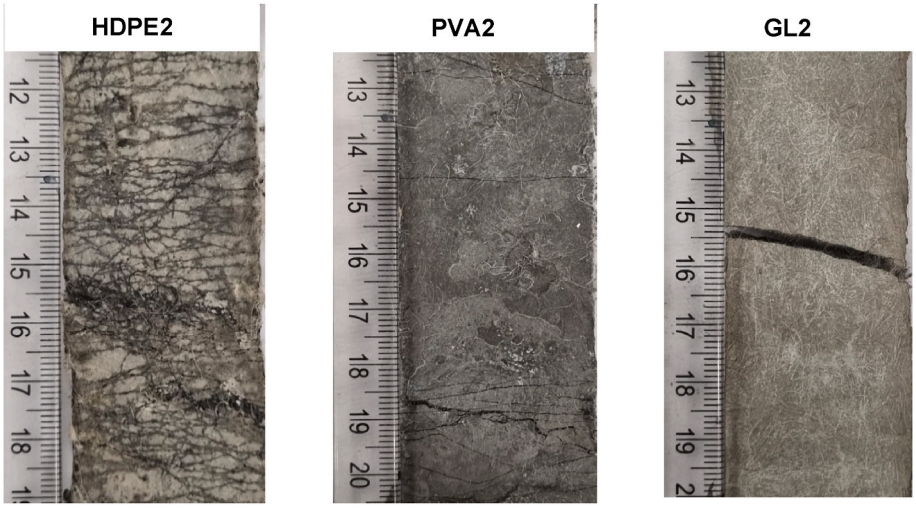

Fig. 5. Typical cracking pattern observed after tensile testing, for different fibre mortars.

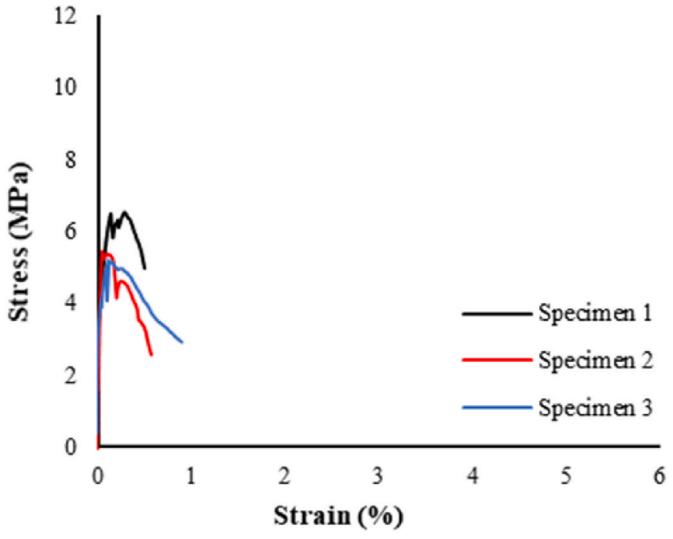

Fig. 6c. GL2.

Table 4
Mechanical parameters of repair mortars.

Mix Nr.	σ_{1st} (MPa)	σ_{max} (MPa)	ε_{max} (%)	$\sigma_{max}/\sigma_{1st}$	$\sigma_{max}/\sigma_{maxPVA2}$
PVA2	3.1 ± 0.6	4.1 ± 0.2	1.80 ± 0.20	1.33	1.00
GL2	4.1 ±1.4	5.5 ± 0.7	0.15 ± 0.02	1.32	1.33
HDPE2	4.6 ±1.3	9.6 ±1.5	4.10 ± 0.60	2.08	2.32

that of the PVA2 and GL2 mix. Furthermore, the strain capacity (ε_{max}) was significantly higher for HDPE2 mix at 4.1%. During the test most of the fibres pulled out instead of breaking. This is because of high fibre strength and hydrophilic nature of these fibres. The bond between fibre and matrix was not more than the tensile strength of the fibres leading to fibre pull-out instead of sudden breakage. The superior tensile properties of these mixes makes them excellent repair materials specially as they can applied in relatively thin layers. These results are in line with the SHCC mixes reported in the literature (Mechtcherine et al., 2011).

3.2. Total shrinkage of repair mortars

The mean values of three test results for total shrinkage of different repair mortars at 1-day intervals are shown in Fig. 7. 0 indicates the starting point of shrinkage measurements which is 24 h after casting. Statistical data with mean and standard deviation (% of mean) for total shrinkage is presented in Fig. 8. The observed standard deviation was found to be always less than ±8 %, which is in-line with standard deviations up to 10% usually reported in shrinkage studies using conventional prism based approach (Melo Neto et al., 2008; Revilla-Cuesta et al., 2022).

Keeping the mix parameters constant, both PVA and glass fibres have a similar effect on shrinkage as the difference is not statistically significant (p-value >0.05). Formulations containing HDPE fibres however showed considerably more total shrinkage. This can be explained by a lower water-cement ratio and presence of higher silica fume content in HDPE formulations. These results are in line with the findings in the literature (Zhang et al., 2003).

Shrinkage curves of cementitious materials can be approximated with various algorithms, among which logarithmic, exponential or hyperbolic functions (Wang et al., 2020; Almudaiheem and Hansen, 1989). Considering the test data presented in Fig. 7(a), a regression analysis was carried out using a hyperbola function as given in Equation (5) to model

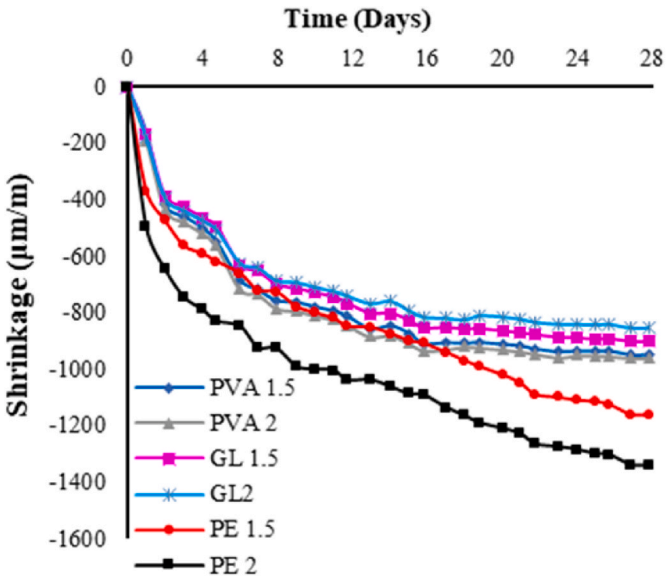

Fig. 7a. Total shrinkage of SHCC.

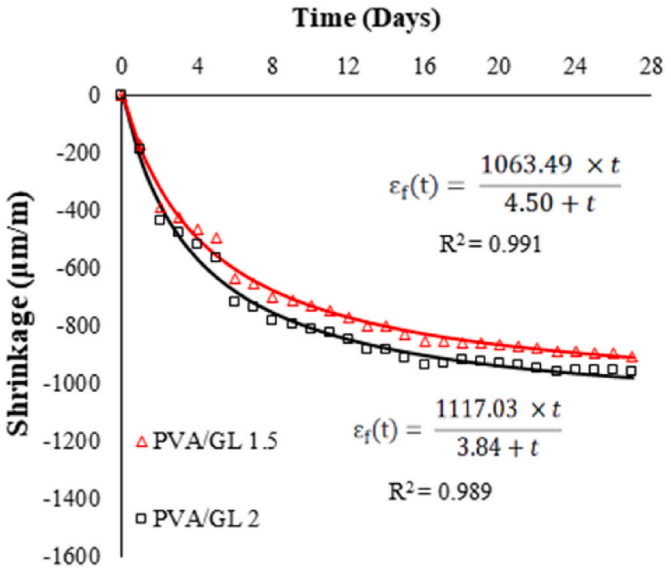

Fig. 7b. PVA/GL mixes regression model.

the selected mix formulations.

$$\varepsilon(t) = \frac{at}{b+t} \tag{5}$$

Where $\varepsilon(t)$ is the shrinkage of the specimen, t is time in days, a is the ultimate shrinkage of the specimen and b corresponds with the time in days when the specimen reaches half of its ultimate shrinkage value. A similar hyperbolic approach is used in ACI 209 (ACI, 2008) (ACI Committee 209, 2092) to predict shrinkage of normal and light weight concrete as it is thought to be convenient for design purposes in which the ultimate value of shrinkage is modified by a time-ratio to get the desired result.

As the shrinkage curves for the PVA and glass fibre mixes are almost identical, the regression analysis on the PVA curves is considered representative for both the PVA and GL types of SHCC tested in this work. Four regression equations are shown in Fig. 7(b) for PVA mixes and Fig. 7(c) for high strength HDPE mixes. The fitting correlation (coefficient of determination R^2) is higher than 0.95 for HDPE

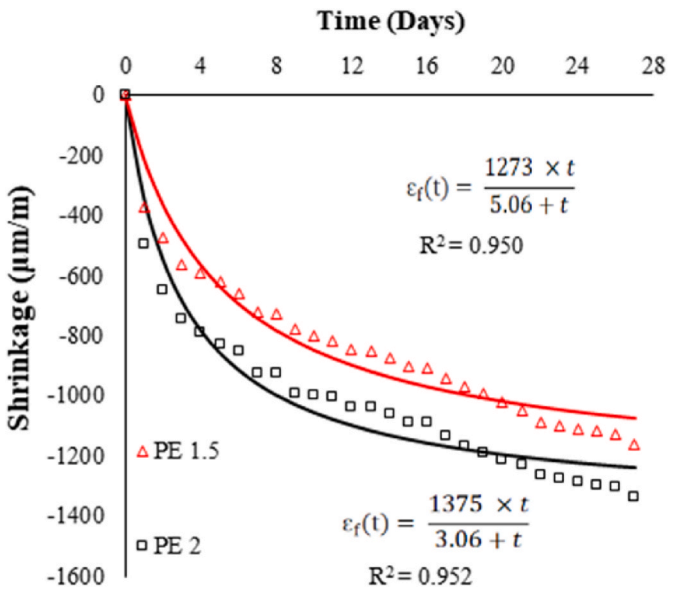

Fig. 7c. HDPE mixes regression model.

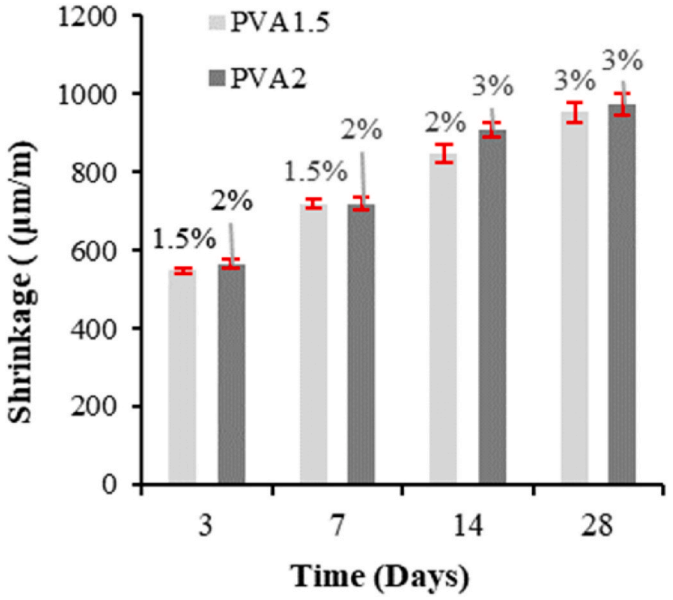

Fig. 8a. HDPE mortars mean values and standard deviation (% of mean).

formulations while it is close to 0.99 for PVA. Summary of the regression coefficients are given in Table 5. Note that the regression analysis extrapolates the recorded data beyond 28 days, so to estimate the final shrinkage (a-value in Eq. (5)) more correctly than assuming the measured value after 28 days.

It can be concluded from the regression equations that the final shrinkage (a) of HDPE and PVA/GL fibre mixes are 1375 µm/m and 1117 µm/m respectively while the time when they reach half of the final shrinkage (b) is 3.1 and 3.8 days. ACI 209 indicates values in the range of 415–1070 µm/m and 20–130 days, for the factors a and b respectively, in reference to normal concrete. These values are however largely dependent on the cured environment and type of mix. As the studied mortars have very low w/b ratio and have no coarse aggregates, higher values are obtained. Wang et al. (2020) performed total shrinkage tests on PVA-SHCC and modelled using similar approach. The final shrinkage value (a) was found out to be 985 µm/m and b as 9.45 days. Compared to the results reported in Fig. 7 and Table 5, the final shrinkage value (a) is

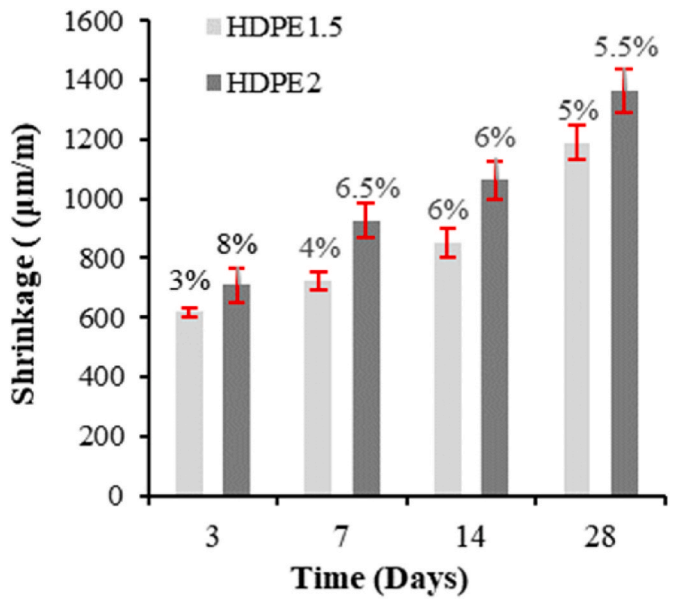

Fig. 8b. HDPE mortars mean values and standard deviation (% of mean).

Table 5
Hyperbolic regression coefficients for total shrinkage of repair mortars.

Mix Nr.	a (µm/m)	b (days)
PVA/GL1.5	1063	4.5
PVA/GL2	1117	3.8
HDPE1.5	1273	5.1
HDPE2	1375	3.1

quite similar, however with a b-value of around 4 days a much faster rate of shrinkage is observed in our study. This can be attributed to the shape of the test specimens (plate type in our study versus traditional prisms in (Wang et al., 2020)), having much more surface area for moisture to evaporate.

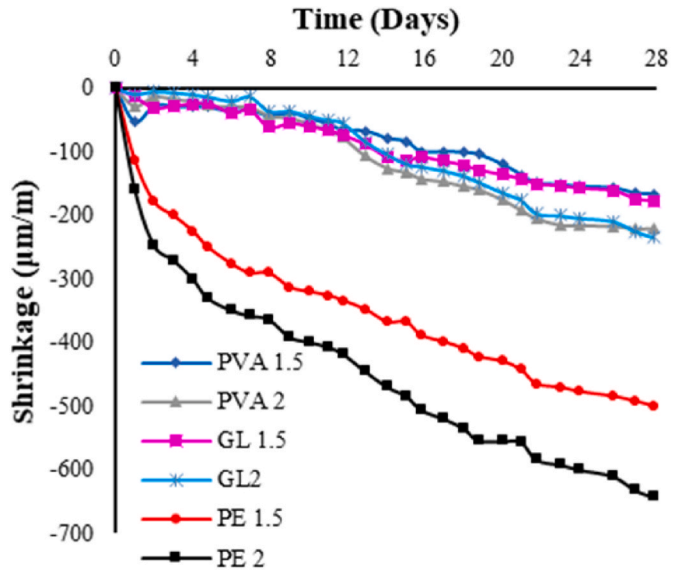

Fig. 9a. Autogenous shrinkage of repair mortars (0 measurement at 28 hours after mixing).

3.3. Autogenous shrinkage of repair mortars

Fig. 9 shows the autogenous shrinkage of all studied formulations recorded from 28 hours after mixing as a function of time for 28 days. Each point represents an average of six data points resulting from three specimens. It is observed for all mixtures that most of the autogenous shrinkage which is attributed to self-desiccation within the concrete composite (Mejlhede Jensen and Freiesleben Hansen, 1996; Snoeck et al., 2015) developed within the first week of hydration. It can be noted that autogenous shrinkage in HDPE fibre formulations was significantly higher than for other fibre mixes (65% increase at 2 vol.-% fibre concentration). Lower autogenous shrinkage in glass and PVA fibre mixes can be explained by the lower cement content, as for these mixes a considerable amount of cement was replaced by FA. The addition of fly ash is known to delay the hydration process contributing to lower autogenous shrinkage (Lee et al., 2015). Furthermore, FA particles have the ability to retain free water due to their spherical particle shape which can also cause a reduction in autogenous shrinkage due to the availability of more free water in the matrix (Şahmaran et al., 2009). On the other hand, in HDPE formulations SF was added which aids in a quick initiation of the pozzolanic reaction. SF reacts with $Ca(OH)_2$ during hydration to produce a dense C–S–H gel which induces high early age autogenous shrinkage (Zhang et al., 2003; Baloch et al., 2019).

An increase of the fibre concentration from 1.5 to 2 vol.-% caused higher autogenous shrinkage, which was observed in all mixes. Even though the absolute value increase was higher in HDPE mixes, a similar relative increase of 22–24% was observed comparing these 2 fibre volume fractions in all mix formulations. Similar results were found in (Meng and Khayat, 2018) on autogenous shrinkage of PVA-SHCC with fibre content greater than 1% and were associated with possible fibre agglomeration in higher fibre content mixes. Autogenous shrinkage was modelled similarly to total shrinkage using a hyperbolic regression model (Equation (5)). The results are indicated in Fig. 9(b) for PVA (also representative for GL) and in Fig. 9(c) for HDPE. For PVA/GL mixes the hyperbolic regression could not be applied and was replaced with a polynomial regression. For the HDPE specimens autogenous shrinkage, the hyperbolic regression remains applicable.

3.4. Drying shrinkage vs autogenous shrinkage

The drying shrinkage of the mixes was calculated by subtracting autogenous shrinkage from total free shrinkage. Fig. 10(a) shows the

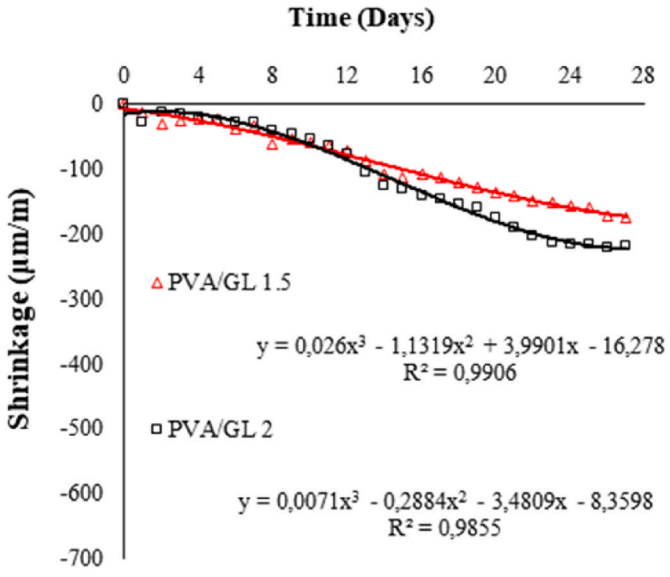

Fig. 9b. PVA/GL mix autogenous shrinkage linear relation.

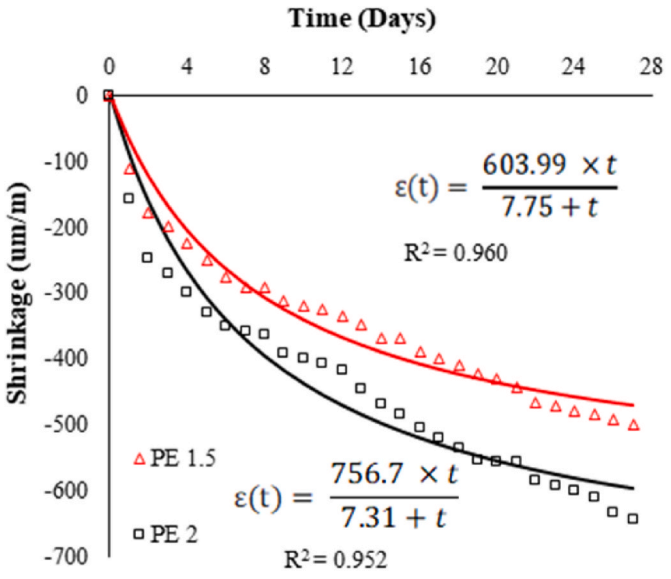

Fig. 9c. HDPE mix autogenous shrinkage hyperbolic relation.

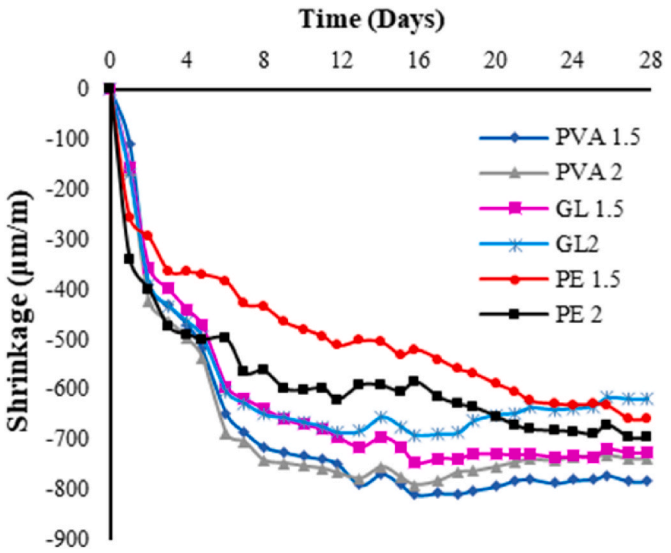

Fig. 10a. Drying shrinkage of repair mortars.

results for all mix formulations studied. Contrary to autogenous shrinkage, drying shrinkage was more pronounced in glass fibre and PVA mixes. This can be explained by a higher water-binder ratio of these mixes compared with the HDPE mixes, as a result of which more water is available for evaporation during curing of the specimens (Liu et al., 2022; Almohammad-albakkar and Behfarnia, 2021).

From practical point of view, it is important to assess the contribution of drying shrinkage compared to autogenous shrinkage as it helps in establishing governing shrinkage mechanism. The autogenous shrinkage of HDPE2 corresponds to 95% of the drying shrinkage at 28 days (Fig. 10 (b)). However for PVA and GL mixes, the contribution of autogenous shrinkage is less significant as it starts at 7 days and corresponds to 25% (Fig. 10(c)) and 30% (Fig. 10(d)) of drying shrinkage, respectively.

3.5. Restrained shrinkage and pull-off bond testing of repair mortars

Fig. 11 shows the average restrained shrinkage development of repair mortar mixes with respect to time. In fact and in reference to Eq. (1) till (3), Fig. 11 shows the measurable free shrinkage part, as the

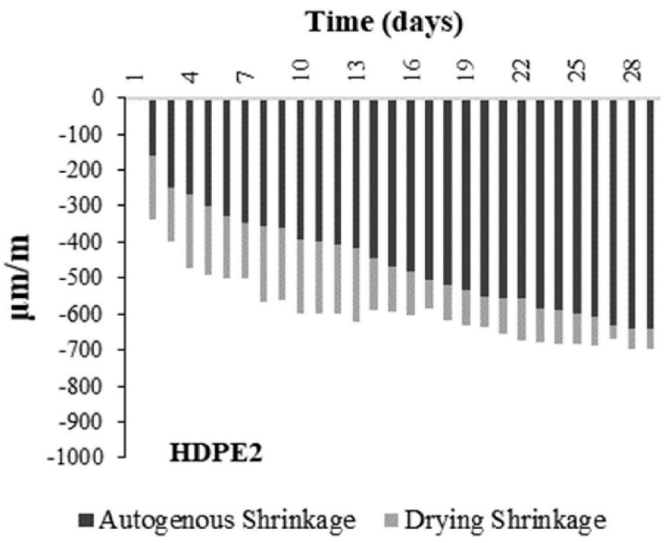

Fig. 10b. Compared graph of autogenous and drying shrinkage of HDPE2.

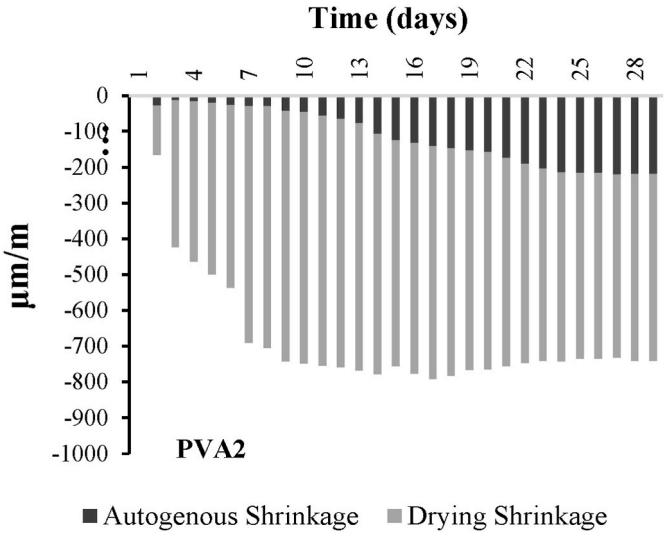

Fig. 10c. Compared graph of autogenous and drying shrinkage of PVA2.

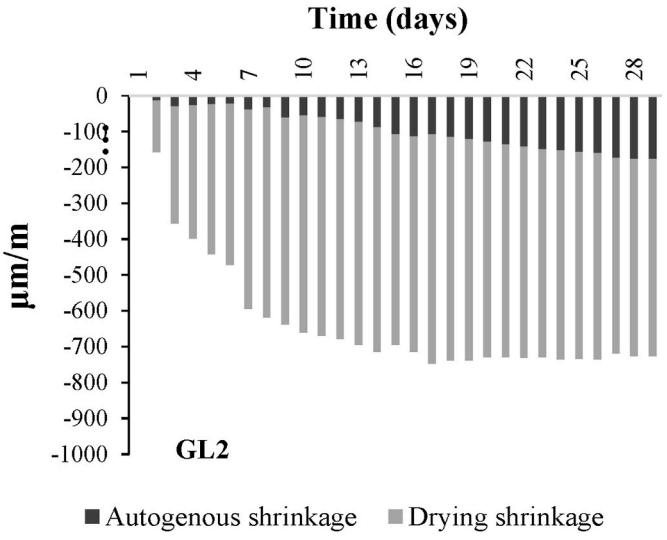

Fig. 10d. Compared graph of autogenous and drying shrinkage of GL2.

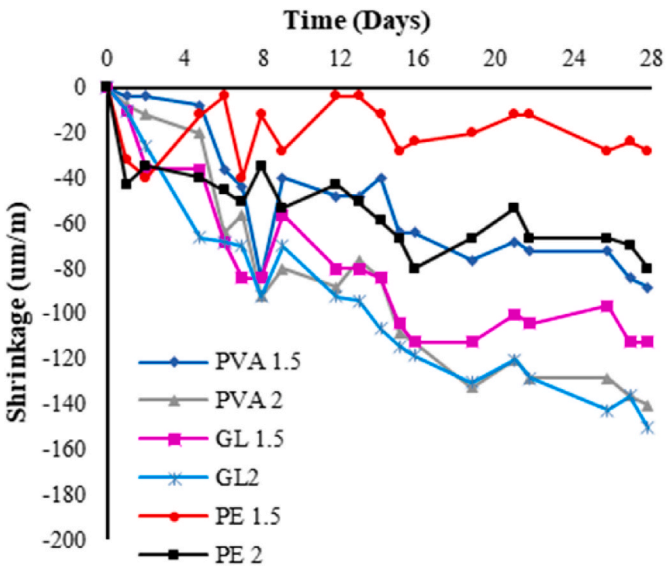

Fig. 11. Restrained shrinkage of repair mortars.

restrained part does not result in a deformation. As a result, it can be noted in Fig. 11 that these values are much smaller compared to total free shrinkage values of the SHCC (Fig. 7), which is expected because of the substrate (that is assumed to almost no longer shrink) restrains the bonded SHCC mortar layer to freely shrink. Due to the restrained shrinkage, shear stresses are generated in the SHCC-substrate bond interface. Nevertheless, no signs of debonding cracking could be observed, indicating proper bond interaction and strength between both materials. Further, the restrained shrinkage is expected to induce tensile stresses in the SHCC mortar layer. There were no visible cracks observed in any of the specimens, while there were few very small cracks (<30 µm) in GL2 and PVA2 samples which could be observed only with magnifiers. The development of restraint strain is also not continuous over time. The used deformeter had a measurement accuracy of 8 µm/m which can explain the fluctuation in these relatively small values that were recorded (Fig. 11). In general, HDPE mixes had the lowest values of shrinkage in restrained conditions, especially HDPE1.5. After 28 days, a value of 28 µm/m is observed for PE1.5, compared to the 150 µm/m for PVA2 and GL2 mixes having the highest values.

3.5.1. Restraint factor over time

The restraint factor (Eq. (2)) for all SHCC mortars versus drying time are plotted in Fig. 12. As the shrinkage values under restrained conditions were very small initially, data is disregarded for the first 7 days. Polynomial regression equations were applied and a moderate correlation $R^2 \approx 0.5$ was obtained. The values of restraint factor varies in the range of 0.92–0.95 for HDPE mixes while they were in the range of 0.82–0.92 for glass and PVA fibre mixes. These high restraint values indicate excellent bond development for all mortars (Abbasnia et al., 2005). The development of the restraint factor in PVA and glass fibre mixes decrease with time and then stabilises after 12 days. Similar behaviour is already reported for restraint factors development of patching repair mortars (Abbasnia et al., 2005) and for concrete (Younis, 2014) in literature. This initial loss of restraint factor can be attributed to the early age micro-cracking observed in PVA and glass fibre mixes which may have reduced the stiffness gain of these mixes (Younis, 2014). On the other hand there is no loss of restraint factor over time for HDPE mixes This again can be explained by the fact that the mix composition of HDPE formulations had a higher cement content and contained silica fume which helps in the early strength gain and in improving the bond behaviour with the substrate.

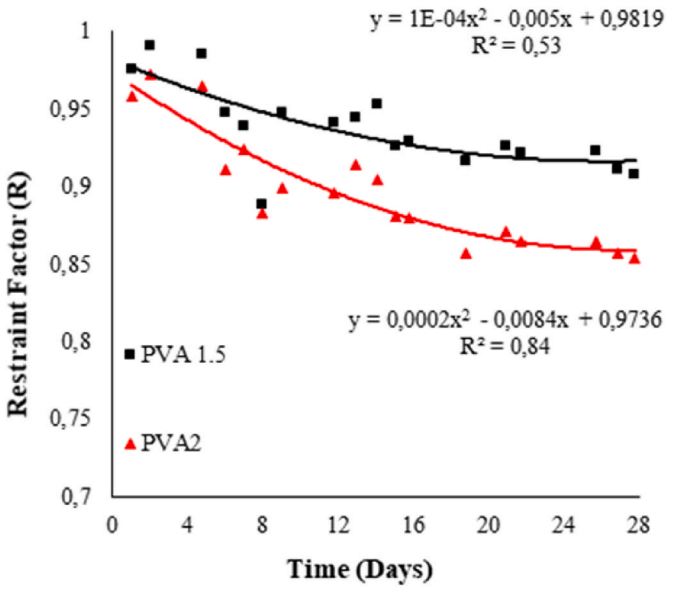

Fig. 12a. PVA fibre mixes.

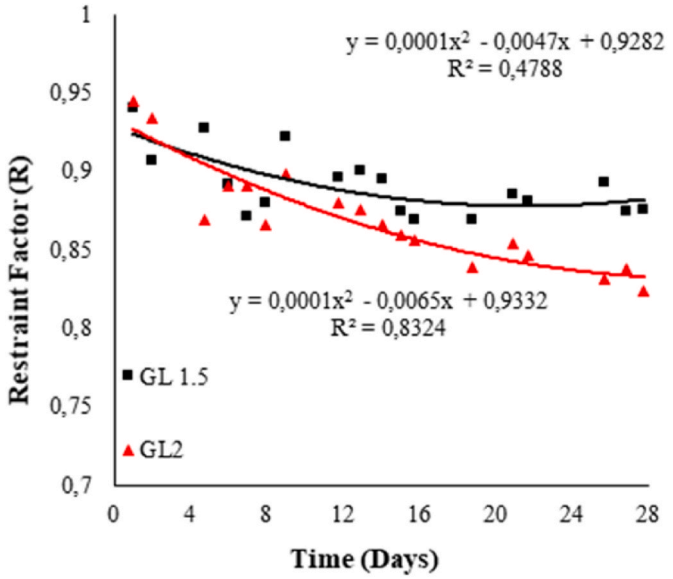

Fig. 12b. Glass fibre mixes.

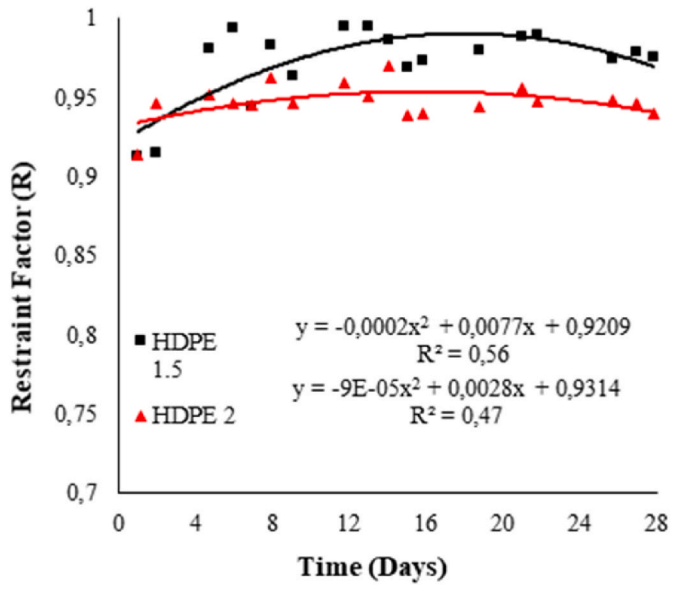

Fig. 12c. HDPE fibre mixes.

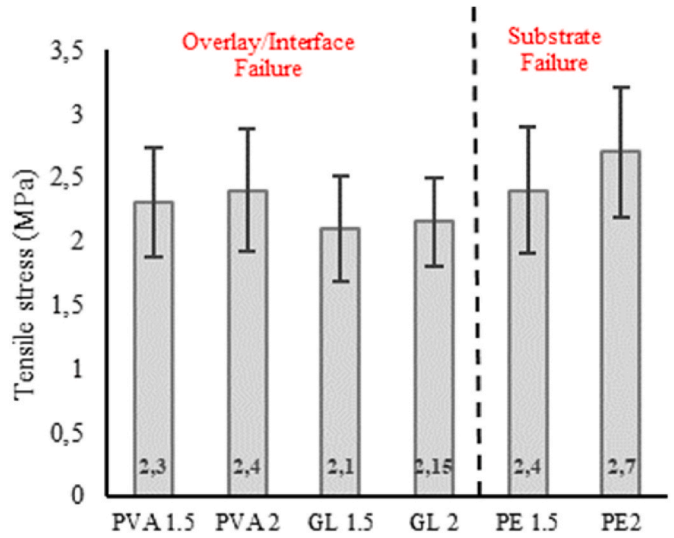

Fig. 13. Pull-off test results of repair mortars.

3.5.2. *Pull-off bond tests*

Pull-off tests were performed on two specimens (and 5 pull-off tests per specimen) for every formulation. Fig. 13 shows the mean of ten data points and the related standard deviation. It is evident from the results that all mixes had more than 2 MPa pull-off bond strength and can be classified as R4 repair mortars according to EN 1542 (BS EN 1542, 1999). It is noted that HDPE mixes performed better as all cores failed in the substrate while it was an overlay/interface failure for the other mixes. In order to fully assess and compare the potential of HDPE mixes, concrete of higher tensile strength must be used. The better bond quality of HDPE mixes might be attributed to the higher cement content and higher tensile strength compared to other mixes. Furthermore, the use of silica fume is also known to increase the bond strength of cementitious composites (Khan and Siddique, 2011). Glass fibre mixes showed slightly lower bond strength than PVA mixes however the difference is not significant. It can be concluded that for the mix designs in this study, the effect of fibre type and concentration had little to no effect on pull-off bond strength.

4. Conclusions

This article reports on the shrinkage and bond behaviour of novel strain hardening fibre-reinforced repair mortars making use of PVA, HDPE or glass fibres. The following conclusions can be drawn from the results.

- PVA and HDPE mortar mixes both showed strain-hardening characteristics as strain capacities were more than 1%. HDPE mixes showed superior properties both in terms of ultimate tensile strength and strain capacity compared with PVA fibre mixes. Glass fibres however showed much less strain capacity at 0.15%, and did not fully classify to be a SHCC. Observation of fracture surface revealed complete breakage of glass fibres which lead to localization of failure instead of continued multiple cracking.
- Both total and autogenous shrinkage were significantly higher in the high strength HDPE fibre formulations compared to glass and PVA

fibre mixes. This can be explained by the usage of higher cement content and use of silica fume instead of fly ash, for the considered strain hardening mix with HDPE fibres.

- Contrary to autogenous shrinkage, drying shrinkage was higher in PVA and glass fibre mixes, compared to the HDPE mix. This is due to the higher water-binder content in these mixes as more water is available for evaporation during the hydration process.
- Bonded to an aged concrete substrate, the shrinkage of the SHCC overlay is restrained to a large extent, as can be expressed by a restraint factor R. For the studied material combinations in this work, R-values at 28 days between 0,83 and 0,94 have been found, associated to the good bond interaction observed. The variation of R at early age is higher and decrease over time.
- Repair mortar layers of restrained shrinkage specimens showed no cracks visible with the naked eye, however, some microcracks were observed using magnifiers. This indicates that the tensile strength of the SHCC overlays could to a large extent accommodate for the stresses induced by the restrained shrinkage. This is also the case for the HDPE SHCC that has higher shrinkage, yet has also higher tensile and strain hardening capacity.
- High strength HDPE mixes showed comparatively better bond quality, which can be attributed to higher cement content and higher tensile strength of these mixes, finally resulting in failure in the concrete substrate.

Declaration of competing interest

The authors declare that they have no known competing financial interests or personal relationships that could have appeared to influence the work reported in this paper.

Data availability

The data that has been used is confidential.

Acknowledgments

The authors would like to acknowledge the financial support provided by the Higher Education Commission (HEC) Pakistan and Ghent University, Belgium.

References

Abbasnia, R., Godossi, P., Ahmadi, J., 2005. Prediction of restrained shrinkage based on restraint factors in patching repair mortar. Cement Concr. Res. 35, 1909–1913. https://doi.org/10.1016/J.CEMCONRES.2004.11.020.

ACI Committee 209. ACI 209.2r-08 guide for modeling and calculating shrinkage and creep in hardened concrete. n.d. https://www.concrete.org/store/productdetail.aspx?ItemID=209208&Format=DOWNLOAD&Language=English&Units=US_AND_METRIC. (Accessed 13 January 2023).

Almohammad-albakkar, M., Behfarnia, K., 2021. Effects of the combined usage of micro and nano-silica on the drying shrinkage and compressive strength of the self-compacting concrete. Journal of Sustainable Cement-Based Materials. https://doi.org/10.1080/21650373.2020.1755382.

Almudaiheem, J.A., Hansen, W., 1989. Prediction of concrete drying shrinkage from short-term measurements. ACI Mater. J. 86, 401–408. https://doi.org/10.14359/2178.

Baloch, H., Usman, M., Rizwan, S.A., Hanif, A., 2019. Properties enhancement of super absorbent polymer (SAP) incorporated self-compacting cement pastes modified by nano silica (NS) addition. Construct. Build. Mater. 203, 18–26. https://doi.org/10.1016/J.CONBUILDMAT.2019.01.096.

Baloch, H., Grünewald, S., Lesage, K., Matthys, S., 2021. Influence of different fibre types on the rheology of strain hardening cementitious composites. In: RILEM Bookseries. Springer Science and Business Media B.V., pp. 3–11. https://doi.org/10.1007/978-3-030-58482-5_1

Beushausen, H., Bester, N., 2016. The influence of curing on restrained shrinkage cracking of bonded concrete overlays. Cement Concr. Res. https://doi.org/10.1016/j.cemconres.2016.05.007.

BS EN 1542, 1999. Products and Systems for the Protection and Repair of Concrete Structures. Test Methods. Measurement of Bond Strength by Pull-Off - European Standards (n.d.). https://www.en-standard.eu/bs-en-1542-1999-products-and-systems-for-the-protection-and-repair-of-concrete-structures-test-methods-measurement-of-bond-strength-by-pull-off/. (Accessed 9 September 2022).

BS EN 1766, 2017. Products and Systems for the Protection and Repair of Concrete Structures. Test Methods. Reference Concretes for Testing - European Standards (n.d.). https://www.en-standard.eu/bs-en-1766-2017-products-and-systems-for-the-protection-and-repair-of-concrete-structures-test-methods-reference-concretes-for-testing/. (Accessed 9 January 2023).

Cheung, A.K.F., Leung, C.K.Y., 2011. Shrinkage reduction of high strength fiber reinforced cementitious composites (HSFRCC) with various water-to-binder ratios. Cement Concr. Compos. 33, 661–667. https://doi.org/10.1016/J.CEMCONCOMP.2011.03.009.

Curosu, I., Liebscher, M., Mechtcherine, V., Bellmann, C., Michel, S., 2017. Tensile behavior of high-strength strain-hardening cement-based composites (HS-SHCC) made with high-performance polyethylene, aramid and PBO fibers. Cement Concr. Res. 98, 71–81. https://doi.org/10.1016/J.CEMCONRES.2017.04.004.

Curosu, I., Muja, E., Ismailov, M., Ahmed, A.H., Liebscher, M., Mechtcherine, V., 2022. An experimental-analytical scale-linking study on the crack-bridging mechanisms in different types of SHCC in dependence on fiber orientation. Cement Concr. Res. 152, 106650 https://doi.org/10.1016/j.cemconres.2021.106650.

Do Yun, H., 2013. Flexural behavior and crack-damage mitigation of plain concrete beam with a strain-hardening cement composite (SHCC) layer at tensile region. Compos. B Eng. 45, 377–387. https://doi.org/10.1016/J.COMPOSITESB.2012.05.053.

Fan, W., Mao, J., Jin, W., Zhang, J., Li, Q., Yuan, F., 2022. Repair effect of cracked reinforced concrete based on electrochemical rehabilitation technology. J. Build. Eng. 61, 105211 https://doi.org/10.1016/j.jobe.2022.105211.

Ghugal, Y.M., Deshmukh, S.B., 2005. Performance of alkali-resistant glass fiber reinforced concrete, 10.1177/0731684405058273. 25 617–630. https://doi.org/10.1177/0731684405058273.

Golias, M., Castro, J., Weiss, J., 2012. The influence of the initial moisture content of lightweight aggregate on internal curing. Construct. Build. Mater. 35, 52–62. https://doi.org/10.1016/j.conbuildmat.2012.02.074.

Hamedanimojarrad, P., Adam, G., Ray, A.S., Thomas, P.S., Vessalas, K., 2012. Development of shrinkage resistant microfibre-reinforced cement-based composites. Cent. Eur. J. Eng. 2, 289–295. https://doi.org/10.2478/S13531-011-0065-Y.

Khan, M.I., Siddique, R., 2011. Utilization of silica fume in concrete: review of durability properties, Resources. Conserv. Recycl. 57, 30–35. https://doi.org/10.1016/J.RESCONREC.2011.09.016.

Khan, M.I., Sial, S.U., Fares, G., ElGawady, M., Mourad, S., Alharbi, Y., 2022. Flexural performance of beams strengthened with a strain-hardening cementitious composite overlay. Case Stud. Constr. Mater. 17, e01645 https://doi.org/10.1016/j.cscm.2022.e01645.

Koch, G., Brongers, M., Thompson, N., Virmani, Y., Payer, J., 2002. Corrosion Costs and Preventive Strategies in the United States, Summary, pp. 1–12.

Lee, H.K., Lee, K.M., Kim, B.G., 2015. Autogenous shrinkage of high-performance concrete containing fly ash, 10.1680/Macr.2003.55.6.507. 55 507–515. https://doi.org/10.1680/MACR.2003.55.6.507.

Li, V.C., 2003. On engineered cementitious composites (ECC). J. Adv. Concr. Technol. 1, 215–230. https://doi.org/10.3151/jact.1.215.

Li, M., Li, V.C., 2006. Behavior of ECC/Concrete Layered Repair System Under Drying Shrinkage Conditions/ Das Verhalten eines geschichteten Instandsetzungssystems aus ECC und Beton unter der. Einwirkung von Trocknungsschwinden 12, 143–160. https://doi.org/10.1515/rbm-2006-6040.

Liu, J., An, R., Jiang, Z., Jin, H., Zhu, J., Liu, W., Huang, Z., Xing, F., Liu, J., Fan, X., Sui, T., 2022. Effects of w/b ratio, fly ash, limestone calcined clay, seawater and sea-sand on workability, mechanical properties, drying shrinkage behavior and micro-structural characteristics of concrete. Construct. Build. Mater. https://doi.org/10.1016/j.conbuildmat.2022.126333.

Mechtcherine, V., 2012. Towards a durability framework for structural elements and structures made of or strengthened with high-performance fibre-reinforced composites. Construct. Build. Mater. 31, 94–104. https://doi.org/10.1016/J.CONBUILDMAT.2011.12.072.

Mechtcherine, V., Millon, O., Butler, M., Thoma, K., 2011. Mechanical behaviour of strain hardening cement-based composites under impact loading. Cement Concr. Compos. 33, 1–11. https://doi.org/10.1016/J.CEMCONCOMP.2010.09.018.

Mejlhede Jensen, O., Freiesleben Hansen, P., 1996. Autogenous deformation and change of the relative humidity in silica fume-modified cement paste. ACI Mater. J. 93, 539–543. https://doi.org/10.1680/adcr.1995.7.25.33.

Melo Neto, A.A., Cincotto, M.A., Repette, W., 2008. Drying and autogenous shrinkage of pastes and mortars with activated slag cement. Cement Concr. Res. 38, 565–574. https://doi.org/10.1016/j.cemconres.2007.11.002.

Meng, W., Khayat, K.H., 2018. Effect of hybrid fibers on fresh properties, mechanical properties, and autogenous shrinkage of cost-effective UHPC. J. Mater. Civ. Eng. 30, 04018030 https://doi.org/10.1061/(asce)mt.1943-5533.0002212.

Ranade, R., Li Prof, V.C., Stults, M.D., Rushing, T.S., Roth, J., Heard, W.F., 2013. Micromechanics of high-strength, high-ductility concrete. ACI Mater. J. 110, 375–384. https://doi.org/10.14359/51685784.

Revilla-Cuesta, V., Evangelista, L., de Brito, J., Skaf, M., Manso, J.M., 2022. Shrinkage prediction of recycled aggregate structural concrete with alternative binders through partial correction coefficients. Cement Concr. Compos. 129, 104506 https://doi.org/10.1016/j.cemconcomp.2022.104506.

Rokugo, K., Yokota, H., Sakata, N., Kanda, T., 2007. Overview of "recommendations for design and construction of high performance fiber reinforced cement composite with multiple fine cracks" published by JSCE. Concrete Journal 45, 3–9. https://doi.org/10.3151/coj1975.45.3_3.

Şahmaran, M., Lachemi, M., Hossain, K.M.A., Li, V.C., 2009. Internal curing of engineered cementitious composites for prevention of early age autogenous shrinkage cracking. Cement Concr. Res. 39, 893–901. https://doi.org/10.1016/J.CEMCONRES.2009.07.006.

Scheerer, S., Schütze, E., Curbach, M., 2018. Strengthening and repair with carbon concrete composites – the first general building approval in Germany. RILEM Bookseries 15, 743–751. https://doi.org/10.1007/978-94-024-1194-2_85/FIGURES/5.

Snoeck, D., Jensen, O.M., De Belie, N., 2015. The influence of superabsorbent polymers on the autogenous shrinkage properties of cement pastes with supplementary cementitious materials. Cement Concr. Res. 74, 59–67. https://doi.org/10.1016/j.cemconres.2015.03.020.

Van Zijl, G.P.A.G., Wittmann, F.H., Oh, B.H., Kabele, P., Toledo Filho, R.D., Fairbairn, E. M.R., Slowik, V., Ogawa, A., Hoshiro, H., Mechtcherine, V., Altmann, F., Lepech, M. D., 2012. Durability of strain-hardening cement-based composites (SHCC). Materials and Structures/Materiaux et Constructions 45, 1447–1463. https://doi.org/10.1617/S11527-012-9845-Y/FIGURES/9.

Wang, S., Li, V., 2005. Polyvinyl alcohol fiber reinforced engineered cementitious composites: material design and performances. Proc., Int'l Workshop on HPFRCC Structural 1–8.

Wang, P., Jiao, M., Hu, C., Tian, L., Zhao, T., Lei, D., Fu, H., 2020. Research on bonding and shrinkage properties of SHCC-repaired concrete beams. Materials 13. https://doi.org/10.3390/MA13071757.

Wei, J., Wu, C., Chen, Y., Leung, C.K.Y., 2020. Shear strengthening of reinforced concrete beams with high strength strain-hardening cementitious composites (HS-SHCC). Materials and Structures/Materiaux et Constructions 53, 1–15. https://doi.org/10.1617/S11527-020-01537-1/FIGURES/12.

Xiong, Y., Yang, Y., Fang, S., Wu, D., Tang, Y., 2021. Experimental research on compressive and shrinkage properties of ECC containing ceramic wastes under different curing conditions. Frontiers in Materials 8, 312. https://doi.org/10.3389/FMATS.2021.727273/BIBTEX.

Xu, W., Jalal, M., Wang, L., 2021. Mechanical and rheological properties of glass fiber-reinforced flowable mortar (GFRFM): optimization using taguchi method. KSCE J. Civ. Eng. 26 (1), 310–324. https://doi.org/10.1007/S12205-021-0502-2, 26 (2021).

Yang, J., Hou, P., Pan, Y., Zhang, H., Yang, C., Hong, W., Li, K., 2021. Shear behaviors of hollow slab beam bridges strengthened with high-performance self-consolidating cementitious composites. Eng. Struct. 242, 112613 https://doi.org/10.1016/J.ENGSTRUCT.2021.112613.

Younis, K.H., 2014. 'Restrained Shrinkage Behaviour of Concrete with Recycled Materials', PhD Thesis. University of Sheffield, Sheffield.

Yu, K., Wang, Y., Yu, J., Xu, S., 2017. A strain-hardening cementitious composites with the tensile capacity up to 8. Construct. Build. Mater. 137, 410–419. https://doi.org/10.1016/j.conbuildmat.2017.01.060.

Zhang, M.H., Tam, C.T., Leow, M.P., 2003. Effect of water-to-cementitious materials ratio and silica fume on the autogenous shrinkage of concrete. Cement Concr. Res. 33, 1687–1694. https://doi.org/10.1016/S0008-8846(03)00149-2.

Zukowski, B., dos Santos, E.R.F., dos Santos Mendonça, Y.G., de Andrade Silva, F., Toledo Filho, R.D., 2018. The durability of SHCC with alkali treated curaua fiber exposed to natural weathering. Cement Concr. Compos. 94, 116–125. https://doi.org/10.1016/J.CEMCONCOMP.2018.09.002.